Solar Energy Materials & Solar Cells 122 (2014) 164–173

Contents lists available at ScienceDirect

Solar Energy Materials & Solar Cells

journal homepage: www.elsevier.com/locate/solmat

Parameters extraction of solar cells – A comparative examination of three methods

J. Appelbaum*, A. Peled

Tel-Aviv University, School of Electrical Engineering, Tel-Aviv 69978, Israel

ARTICLE INFO

Article history:
Received 16 September 2013
Accepted 5 November 2013
Available online 28 December 2013

Keywords:
Parameters extraction
Newton–Raphson
Levenberg–Marquardt
Lambert-W function
Genetic Algorithm
Si and MJ solar cells

ABSTRACT

This paper deals with the extraction of the parameters of the single-diode solar cell model from experimental I–V characteristics of Si and Multi-junction solar cells. The extraction is carried out by three different optimization methods in an attempt to judge which method surpasses the others in terms of data-to-model fitting. The first and the second methods are a variation of the Newton-Raphson method and the Levenberg–Marquardt algorithm, respectively. Both methods are based on the gradient descent approach. The third method is a global-search method based on a Genetic-Algorithm. The extraction of the parameters was done in two stages. On the first stage, empirical I–V characteristics of solar cells that contained measurement errors were used, whereas on the second stage the parameters were re-extracted using a smooth synthetic I–V data. In the absence of true measured parameter values of the cells, it was left to rate the performance of the three optimization methods by the extraction error alone. Although no definitive conclusions could be drawn from the results of the noisy data, results of the smooth data are far more pronounced in terms of the extraction error, and tend to favor the Newton-Raphson method.

1. Introduction

Formulating an equation that describes the performance of photovoltaic cells under illumination or in dark conditions, one from which the cell's physical parameters can be restored, is of great value in the field of photovoltaic engineering. The single-diode model that describes the cell's current–voltage relationship is basically derived from the semiconductor equations that govern the physics of solar cells. Once a solar cell model has been established, optimization methods can be employed to extract the unknown model parameters. Each parameter accounts for a different component that constitutes the electrical circuitry of the model. The one-diode model shown in Fig. 1(a), is composed of 5 such parameters, namely the series and the shunt resistance, R_s and R_{sh}, respectively, the diode ideality factor n, the diode reverse-saturation current I_0, and the photogenerated current I_L.

Although the one-diode model is considered accurate, it is oftentimes elaborated in order to follow the behavior of solar cells more adequately. Ben-Or et al. [1] extended the set of conventional parameters in the one-diode model, to include 8 parameters instead of 5. By adding to the model α, V_{br} and m – the cell's correction coefficient, breakdown voltage and exponent-power, respectively, the model was extended to cover the cell's negative-voltage operation mode.

The act of parameters extraction, may be perceived as being subjected to two opposing aspects, mathematical and physical. On the one hand, the problem of combining a model with an experimental data so as to extract its parameters is purely mathematical. From the mathematical point of view, it is apparently favorable to employ a model that consists of a small number of parameters, one which reduces the complexity level of optimization. On the other hand, from the physical point of view it may be unrealistic to confine ourselves to the one-diode model, since parametric-wise, an extended model covers a larger number of phenomena that underlie the physics of solar cells. This in turn enhances the accuracy of the model. (See: Fig. 1(b) - the two-diode model)

The parameters extraction has an extensive reference in the related literature. It can be claimed that the extraction procedures are distinguished by the amount of the data samples that participate in the extraction procedure, by the type of model being used, and by the mathematical approach that is employed. Focusing on the mathematical aspect, the parameters extraction of solar cells is generally divided into two categories – numerical methods and analytical methods. Numerical methods rely on curve fitting algorithms to find an optimized fit between theoretical and experimental I–V characteristics of solar cells. These curve fitting methods are said to have an overall higher level of confidence in

* Corresponding author.
E-mail address: appel@eng.tau.ac.il (J. Appelbaum).

0927-0248/$ - see front matter Crown Copyright © 2013 Published by Elsevier B.V. All rights reserved.
http://dx.doi.org/10.1016/j.solmat.2013.11.011

Nomenclature

ACT	algorithm conversion time
I_0	diode reverse saturation current
I_L	solar cell's photogenerated current
I_{sc}	solar cell's short-circuit current
n	diode ideality factor
R_{sh}	solar cell model's shunt resistance
R_s	solar cell model's series resistance
V_{oc}	solar cell's open-circuit Voltage
V_T	thermal voltage
GA	Genetic-Algorithm
LMA	Levenberg–Marquardt Algorithm
MJ	multi-junction
NRM	Newton–Raphson Method

terms of the resulting values of the parameters, since the majority or the entire set of I–V samples are used throughout the extraction procedure. On the other hand, the accuracy of the fitting methods depends on the type of the method, the objective function to be minimized, and the starting values of the parameters that are introduced prior to the running of the algorithm. In addition, curve fittings that are based on gradient-descent methods may tend to converge to local rather than global extrema on account of an inappropriate choice of initial values. Also, these methods may require a relatively long computation time. In contrast, analytical methods only require a limited set of I–V points corresponding to a finite set of equations whose solution are the parameter values. In that sense, analytical methods are characterized by a straightforward algebraic approach. Bearing in mind, however, that experimental I–V samples may contain measurement errors makes it vital to choose an appropriate set of points in order to avoid inaccuracy.

Various parameters extraction techniques have been proposed in the literature, and since the parameters extraction is a multidimensional numerical optimization problem, different authors have obtained different values of parameters for common sets of I–V data. Therefore it can be argued that no method insures completely reliable results for the extracted parameters. Ghani and Duke [2] proposed an approach whereby only R_s and R_{sh} are extracted, relying solely on the maximum power-point values of the voltage and the current. The experimental I_m and V_m in [2] were retrieved from a relevant manufacturer datasheet. The resistances were extracted by applying the Newton–Raphson technique to find the roots of an equation that was derived from the single-diode model. Chan et al. [3] have also used the Newton–Raphson technique to minimize the error difference, denoted $\Delta Area$, between the areas confined under the empirical and theoretical I–V curves. In [3], two types of extraction are presented – the 5-point

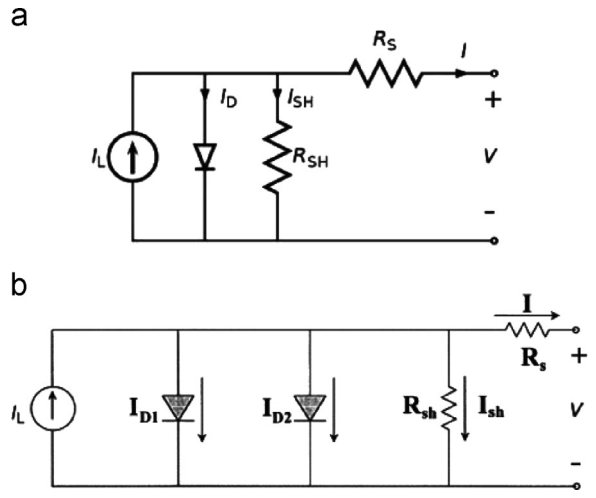

Fig. 1. An equivalent electrical circuit of a solar cell under illumination: (a) The single-diode model, and (b) The two-diode model.

method, whereby 5 equations are solved for 5 distinct points along the I–V curve, and a Newton–Raphson based curve-fitting technique, where the entire set of data points is used. Appelbaum et al. [4] have suggested a new approach to sort an array of solar cells based on their performance. The procedure in [4] involved the use of the single and the two-diode models. Parameters extraction via a quasi-Newton based curve fitting was demonstrated in [4] on a batch of 50 silicon solar cells. Yadir et al. [5] used the same error criterion as in [3] but obtained the analytical expression for the area under the I–V curve through derivation of the single-diode model equation.

Ye et al. [6] applied the particle swarm optimization and the genetic-algorithm methods on both synthetic and experimental I–V data, using the two-diode and the single-diode models. The second diode in the two-diode model contributes two additional parameters-an ideality factor n_2 and a reverse saturation current I_{02}, The latter is typically 10^5 times smaller than its counterpart, I_{01}. In terms of the objective-function minimization, the results for the two-diode were slightly improved in comparison to the one-diode model. Maoucha et al. [7] too, have used a Trust-Region based optimization to extract the seven parameters of the two-diode model for measured data of organic solar cells. Chan et al. [8] used the two-diode model and applied the Newton–Raphson method to extract parameters from silicon cells. Algebraic substitutions were used in [8] to reduce the number of the extracted parameters.

This paper focuses on three methods of parameters extraction, of which the first two are gradient-descent based techniques, hence local in their search. The third method, a genetic algorithm based extraction, is global in its search and requires no initial values for the parameters. In this work, we restrict ourselves to the single-diode model. We first reduce the cell model to three parameters instead of five, by using some algebraic manipulations. The objective function that is derived from the reduced model is then applied to all three methods. The first Newton–Raphson Method (NRM) that was used in several other works has been altered here by adding an additional stage in between the traditional steps of the algorithm. This variation was carried out in order to overcome some convergence difficulties arising from the complex nature of the objective function. The two other methods, namely the Levenberg–Marquardt Algorithm (LMA) and the Genetic-Algorithm (GA), were left unchanged. All extraction methods were examined on three Si cells as well as on a Multi-junction cell with concentration of 350, 555 and 750 Sun. In the Si cells case, the extraction was mainly performed in order to show that the extracted values bear similarities to the expected physical parameters which characterize Si cells. In the multi-junction cell case, we expected the value of the extracted parameters to show correspondence with the increasing of the concentration level.

2. The single-diode and the two-diode model equations

Under Illumination, the I–V characteristics of a p–n junction solar cell at forward-bias, can be represented by the following

single-diode model equation:

$$I(V) = I_L - I_0 \cdot \left(\exp\left(\frac{V + I \cdot R_s}{n \cdot V_T}\right) - 1\right) - (V + I \cdot R_s)/R_{sh} \tag{2.1}$$

In Eq. (2.1), I_L denotes the photogenerated current. The parasitic resistances, R_s and R_{sh}, represent the ohmic losses in the semiconductor bulk and in the metallic contacts, and the current leakages across the p-n junction, respectively. The diode (whose current is denoted I_D) in Fig. 1(a) contributes to Eq. (2.1) the exponential term which includes I_0 – the diode's reverse saturation current, n – the diode's ideality factor, and V_T – the thermal voltage. It should be noted that I_0 and n both depend on the properties of the cell's semiconductor material, and that the latter provides information on the quality of the junction.

When an experimental I–V data is provided, it is possible to transform Eq. (2.1) into a 3-parameters equation by a substitution of some of the parameters with algebraic expressions. At the short-circuit point of the solar cell, Eq. (2.1) gives

$$V = 0, \quad I = I_{sc} \Rightarrow I_{sc} = I_L - I_0 \cdot \left(\exp\left(\frac{I_{sc} \cdot R_s}{n \cdot V_T}\right) - 1\right) - I_{sc} \cdot R_s/R_{sh} \tag{2.2}$$

Similarly, at the solar cell's open-circuit point, we have

$$V = V_{oc}, I = 0 \Rightarrow 0 = I_L - I_0 \cdot \left(\exp\left(\frac{V_{oc}}{n \cdot V_T}\right) - 1\right) - V_{oc}/R_{sh} \tag{2.3}$$

The solar cell short-circuit I_{sc}, and open-voltage V_{oc}, can be obtained from the experimental I–V curve by linear approximation around $V=0$ and $V = V_{oc}$. Solving (2.2), (2.3) for I_L and I_0, we get

$$I_0 = \frac{[I_{sc}(1 + R_s/R_{sh}) - V_{oc}/R_{sh}] \cdot \exp\left(-\frac{V_{oc}}{n \cdot V_T}\right)}{1 - \exp\left(\frac{R_s \cdot I_{sc} - V_{oc}}{n \cdot V_T}\right)} \tag{2.4}$$

$$I_0 + I_L = \frac{I_{sc}(1 + R_s/R_{sh}) - V_{oc}/R_{sh}}{1 - \exp\left(\frac{R_s \cdot I_{sc} - V_{oc}}{n \cdot V_T}\right)} + V_{oc}/R_{sh} \tag{2.5}$$

Therefore, substituting Eqs. (2.4), (2.5) into Eq. (2.1), the terms I_0 and I_L are eliminated, and Eq. (2.1) can thereafter be re-written as

$$I = \frac{V_{oc} - V - I \cdot R_s}{R_{sh}} - \frac{[I_{sc}(1 + R_s/R_{sh}) - V_{oc}/R_{sh}] \cdot \left(\exp\left(-\frac{V_{oc} - V - I \cdot R_s}{n \cdot V_T}\right) - 1\right)}{1 - \exp\left(\frac{R_s \cdot I_{sc} - V_{oc}}{n \cdot V_T}\right)} \tag{2.6}$$

The second model, also known as the two-diode model [6,9,10], is used to simulate the space charge recombination effect by incorporating a separate current component with an exponential term. Thus, the two-diode model enables to gain further insight into the physical phenomena inside the cell, and is often claimed to be more accurate than the single-diode model. The I–V relationship of the two-diode model whose equivalent electrical circuit appears in Fig. 1(b) is described as follows:

$$I(V) = I_L - I_{01} \cdot \left(\exp\left(\frac{V + I \cdot R_s}{n_1 \cdot V_T}\right) - 1\right) - I_{02} \cdot \left(\exp\left(\frac{V + I \cdot R_s}{n_2 \cdot V_T}\right) - 1\right) - (V + I \cdot R_s)/R_{sh} \tag{2.7}$$

where, as stated before, I_{01} and I_{02} denote the diffusion and recombination characteristics of the charge carriers in the material and in the space-charge region of the cell, respectively. Likewise, n_1 and n_2 are the diffusion and recombination diode ideality factors, respectively. Other variables in Eq. (2.7) are similar to those of Eq. (2.1). It is well established [10] that I_{01} is typically 10^5 times greater than I_{02}, a fact that may favor the restriction to the single-diode model. Secondly, it is often assumed in the literature [7,9] that the ideality factor values are constant, namely $n_1 = 1$ and $n_2 = 2$. In that sense, the ideality factor in Eq. (2.1) represents an equivalent ideality factor that encompasses the physical phenomena inside the cell, and whose value lies somewhere between 1 and 2. Assigning the ideality factors constant values in Eq. (2.7), the number of unknown parameters is reduced from 7 to 5:

$$I(V) = I_L - I_{01} \cdot \left(\exp\left(\frac{V + I \cdot R_s}{V_T}\right) - 1\right) - I_{02} \cdot \left(\exp\left(\frac{V + I \cdot R_s}{2 \cdot V_T}\right) - 1\right) - (V + I \cdot R_s)/R_{sh} \tag{2.8}$$

At the short-circuit and open-circuit points, Eq. (2.8) gives

$$I_{sc} = I_L - I_{01} \cdot (\exp(I_{sc} \cdot R_s/V_T) - 1) - I_{02} \cdot (\exp(I_{sc} \cdot R_s/(2 \cdot V_T)) - 1) - I_{sc} \cdot R_s/R_{sh} \tag{2.9}$$

$$0 = I_L - I_{01} \cdot (\exp(V_{oc}/V_T) - 1) - I_{02} \cdot (\exp(V_{oc}/(2 \cdot V_T)) - 1) - V_{oc}/R_{sh} \tag{2.10}$$

Re-arranging Eqs. (2.9), (2.10) and using a matrix notation, we get

$$\begin{bmatrix} I_{01} \\ I_{02} \end{bmatrix} = \begin{bmatrix} \exp(I_{sc} \cdot R_s/V_T) - 1 & \exp(I_{sc} \cdot R_s/(2V_T)) - 1 \\ \exp(V_{oc}/V_T) - 1 & \exp(V_{oc}/(2V_T)) - 1 \end{bmatrix}^{-1} \begin{bmatrix} I_L - I_{sc}(1 + R_s/R_{sh}) \\ I_L - V_{oc}/R_{sh} \end{bmatrix} \tag{2.11}$$

Solving the system in Eq. (2.11), it can be verified that

$$I_{01} = \frac{I_L - I_{sc} \cdot (1 + R_s/R_{sh})}{\left(\exp\left(\frac{V_{oc}}{2V_T}\right) - 1\right)\left(\exp\left(\frac{I_{sc} \cdot R_s}{2V_T}\right) - \exp\left(\frac{V_{oc}}{2V_T}\right)\right)} - \frac{I_L - V_{oc}/R_{sh}}{\left(\exp\left(\frac{V_{oc}}{2V_T}\right) - 1\right)\left(\exp\left(\frac{I_{sc} \cdot R_s}{2V_T}\right) - \exp\left(\frac{V_{oc}}{2V_T}\right)\right)} \tag{2.12}$$

$$I_{02} = \frac{[I_{sc} \cdot (1 + R_s/R_{sh}) - I_L]\left(\exp\left(\frac{V_{oc}}{2V_T}\right) + 1\right)}{\left(\exp\left(\frac{I_{sc} \cdot R_s}{2V_T}\right) - 1\right)\left(\exp\left(\frac{I_{sc} \cdot R_s}{2V_T}\right) - \exp\left(\frac{V_{oc}}{2V_T}\right)\right)} - \frac{(I_L - V_{oc}/R_{sh})\left(\exp\left(\frac{I_{sc} \cdot R_s}{2V_T}\right) + 1\right)}{\left(\exp\left(\frac{V_{oc}}{2V_T}\right) - 1\right)\left(\exp\left(\frac{I_{sc} \cdot R_s}{2V_T}\right) - \exp\left(\frac{V_{oc}}{2V_T}\right)\right)} \tag{2.13}$$

Substituting Eqs. (2.12), (2.13) into Eq. (2.7), the number of parameters in Eq. (2.7) is reduced from 5 to 3. Parameters extraction from the two-diode model is beyond the scope of this paper. However, this model together with Eqs. (2.12) and (2.13) may serve as a basis for a further development in the future.

3. Determining the parameters initial values

The initial values assigned to the extracted parameters affect the convergence of the NRM and the LMA methods. Setting the initial values for the parameters requires first an estimation of the short-circuit current and the open-circuit voltage, each of which is obtained from the experimental I–V characteristics by means of linear regression around those two endpoints. Having two polynomials derived from the linear regressions, I_{sc} is then determined as the interception of the first polynomial with the vertical I-axis, whereas V_{oc} is determined from the second polynomial's interception with the horizontal V-axis. Formally speaking, denoting the first and the second polynomials $I_1 = a_1 + b_1 V$ and $I_2 = a_2 + b_2 V$, respectively, we have:

$$I_{sc} = a_1, V_{oc} = -a_2/b_2 \tag{3.1}$$

The initial values of the series resistance, $R_s^{(0)}$ and the shunt resistance, $R_{sh}^{(0)}$, are evaluated around the open-circuit and the

short-circuit points, respectively. Taking the derivative of Eq. (2.1) with respect to V, and re-arranging the resulting expression, we have:

$$\frac{dI}{dV}=\frac{-1/R_{sh}}{1+R_s/R_{sh}+I_0\cdot R_s/(n\cdot V_T)\cdot\exp\left(\frac{V+I\cdot R_s}{n\cdot V_T}\right)} \tag{3.2}$$

where the term R_s/R_{sh} may be neglected from Eq. (3.2) since it is assumed that $R_{sh}\gg R_s$. It follows from Eq. (3.2) that at the short-circuit point

$$\frac{dI}{dV}=\frac{-1/R_{sh}}{1+(I_0\cdot R_s/(n\cdot V_T))\cdot\exp\left(\frac{I_{sc}\cdot R_s}{n\cdot V_T}\right)}.$$

However, since it is generally true that

$$\frac{I_0\cdot R_s}{n\cdot V_T}\cdot\exp\left(\frac{I_{sc}\cdot R_s}{n\cdot V_T}\right)\ll 1$$

(which can be easily verified upon substituting typical values into the left-hand side of the inequality), we have: $(dI/dV)_{I_{sc}}=-1/R_{sh}$. Bearing in mind that $(dI/dV)_{I_{sc}}=b_1$, it follows that $R_{sh}=|1/b_1|$. Likewise, at the open-circuit point:

$$\frac{dI}{dV}=\frac{-1/R_{sh}}{1+I_0\cdot R_s/(n\cdot V_T)\cdot\exp\left(\frac{V_{oc}}{n\cdot V_T}\right)}.$$

Having $(dI/dV)_{V_{oc}}=b_2$ and re-arranging the latter derivative expression, it is possible to isolate R_s. Also, as a rule of thumb, the diode-ideality factor, n, is equal 1.5 for Si cells and 2.5 for MJ cells. The initial values are summarized below.

$$R_{sh}^{(0)}=\left|\frac{1}{b_1}\right|,R_s^{(0)}=\left|\left(\frac{-1}{R_{sh}^{(0)}\cdot b_2}-1\right)\frac{n^{(0)}\cdot V_T}{I_0^{(0)}}\cdot\exp\left(-\frac{V_{oc}}{n^{(0)}\cdot V_T}\right)\right| \tag{3.3}$$

$$n^{(0)}=\begin{cases}1.5 & \text{(for Si cells)}\\ 2.5 & \text{(for MJ cells)}\end{cases} \tag{3.4}$$

4. Parameters extraction with an extended version of the Newton–Raphson method

In numerical analysis, the Newton–Raphson method is used for finding successfully better approximations to the roots of a real-valued function . Given a function $f(x)$ defined over x, and its derivative f', the search begins with an initial guess x_0 for a root of f. Provided that the function satisfies all the assumptions made in the derivation of the formula, the process is repeated, so that the approximation x_n in the nth iterative step is

$$x_n=x_{n-1}-\frac{f(x_{n-1})}{f'(x_{n-1})} \tag{4.1}$$

The formula in Eq. (4.1) can be easily implemented for finding a local extremum value $\hat{x}$ of $f(x)$. Since $\hat{x}$ is a root of $f'(x)$, Eq. (4.1) should be altered as follows:

$$\hat{x}_n=\hat{x}_{n-1}-\frac{f'(x_{n-1})}{f''(x_{n-1})} \tag{4.2}$$

In the *multidimensional* case where $\underline{\hat{x}}=[x_1,x_2,\ldots,x_m]$, Eq. (4.2) is modified as

$$\underline{\hat{x_n}}=\underline{x_{\hat{n-1}}}-\underline{\underline{H}}^{-1}(\underline{x_{\hat{n-1}}})\cdot\underline{g}(\underline{x_{\hat{n-1}}}) \tag{4.3}$$

where in Eq. (4.3), $\underline{\underline{H}}$ is the Hessian square matrix of the function $f(\underline{x})$, such that any element of $\underline{\underline{H}}$ is given by

$$H_{i,j}=\left(\frac{\partial^2 f(\underline{x})}{\partial x_i\partial x_j}\right)_{\underline{x}=\underline{\hat{x_n}}},$$

and $\underline{g}$ is the gradient column vector of $f(\underline{x})$, whose ith element is $g_i=(\partial f/\partial x_i)_{\underline{x}=\underline{\hat{x_n}}}$.

Back to our topic, we denote $\underline{\beta}$ the vector of unknown parameters, namely $\underline{\beta}=[R_s,R_{sh},n]$, considering the 3-parameters model in Eq. (2.6). An objective function $S(\underline{\beta},I_{sc},V_{oc})$ is defined over $\underline{\beta}$, as the squared difference between the experimental and the theoretical data:

$$S(\underline{\beta},I_{sc},V_{oc})=\sum_{k=1}^{N}(I_k^{exp}-I_k^{th})^2 \tag{4.4}$$

where I_k^{exp} is the kth sample out of N experimental current data samples. Likewise, I_k^{th} is the kth sample of the theoretical current, subjected to Eq. (2.6):

$$I_k^{th}=\frac{V_{oc}-V_k^{exp}-I_k^{exp}\cdot R_s}{R_{sh}}-\frac{[I_{sc}(1+R_s/R_{sh})-V_{oc}/R_{sh}]\cdot\left(\exp\left(-\frac{V_{oc}-V_k^{exp}-I_k^{exp}\cdot R_s}{n\cdot V_T}\right)-1\right)}{1-\exp((R_s\cdot I_{sc}-V_{oc})/(n\cdot V_T))} \tag{4.5}$$

Substituting $\underline{\beta}$ into Eq. (4.3), gives the Newton–Raphson iterative process which optimizes f with respect to $\underline{\beta}$:

$$\underline{\beta_n}=\underline{\beta_{n-1}}-\underline{\underline{H}}^{-1}(S)_{\underline{\beta}=\underline{\beta_{n-1}}}\cdot\underline{g}(S)_{\underline{\beta}=\underline{\beta_{n-1}}} \tag{4.6}$$

Narrowing the search for 3 parameters instead of 5, enables the visualization the objective function, S, in the three-dimensional space, which in turn assists to gain an insight into the objective function's behavior. This proves to be vital in the analysis of the Multi-junction cells, where the Newton–Raphson iterative process oftentimes has a tendency to diverge. Fig. 3 exemplifies the visualization of the objective function of a Multi-junction cell under a concentration of 555 Sun whose I–V characteristics can be seen in Fig. 2. The MJ cell values of short-circuit current and the open-circuit voltage were found to be 7.0733A and 2.9581 V, respectively. Both values were obtained from the cell's I–V characteristics, with the aid of Eq. (3.1).

In Fig. 3(a), the objective function S related to the MJ cell is projected onto the three-dimensional space characterized with $R_s=0.02[\Omega]$. Likewise, in Fig. 3(b) the objective function is projected onto the $R_s=0.04[\Omega]$−space. The two horizontal axes in Fig. 3(a) and (b), namely the shunt-resistance R_{sh}, and the diode ideality factor n, span from 20 to 100 Ω, and from 2 to 3, respectively. Although the figures exhibit different profiles with respect to R_s, it is evident in both figures that S varies slightly with

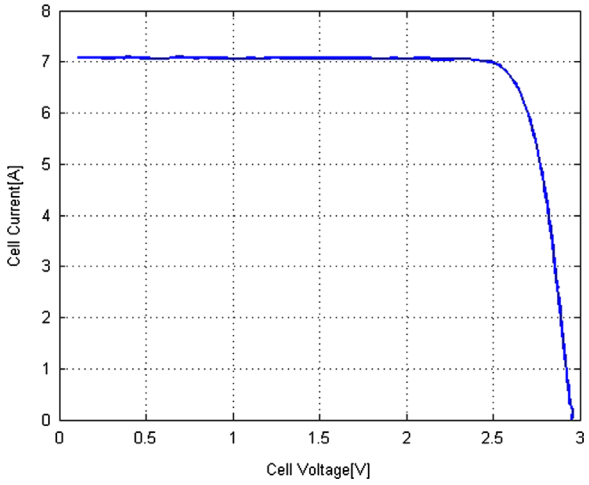

Fig. 2. A Multi-junction cell's I–V characteristics.

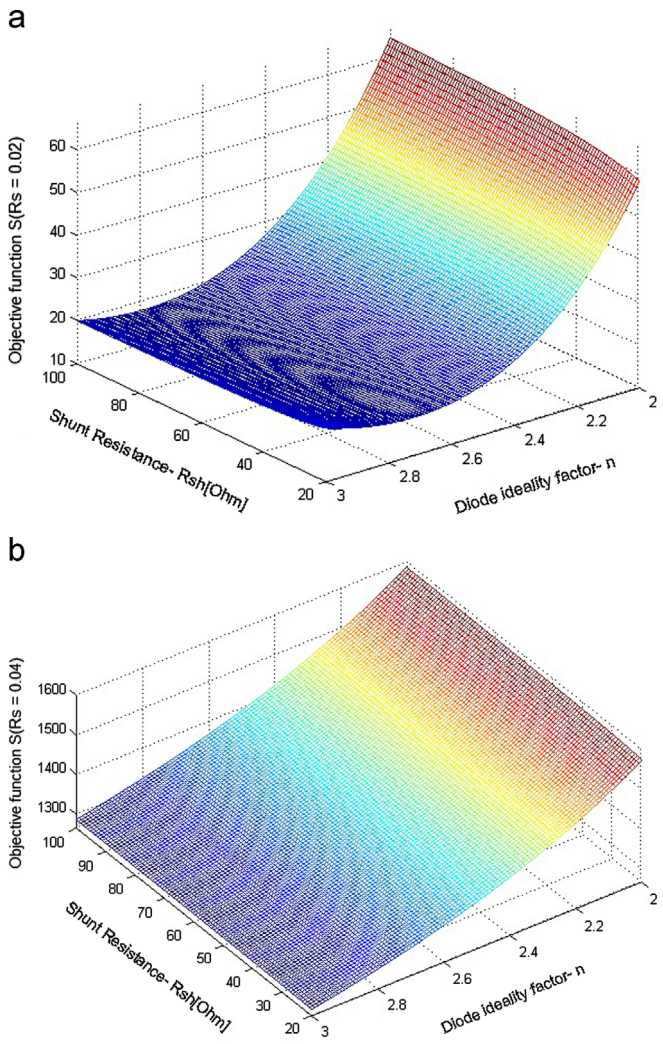

Fig. 3. Visualization of the objective function $S(\beta, I_{sc}, V_{oc})$: (a) f projected onto $R_s = 0.02[\Omega]$ space, and (b) f projected onto $R_s = 0.04[\Omega]$ space.

respect to R_{sh}, whereas it has a strong dependence on the value of n. In Fig. 3(a), the convex shape of $S(0.02, R_{sh}, n)$ clearly shows that a minimum value is obtained somewhere around $n=2.7$. A more accurate examination reveals that S achieves a minimum value of 17.93 at $R_{sh} = 100, n = 2.788$. It is worth mentioning that at the point of boundary, $R_{sh} = 20, n = 2.788$, f only increases to 19.05, affirming the weak dependence of S on R_{sh}. A similar examination of $f(0.04, R_{sh}, n)$ as shown in Fig. 3(b) yields the extremum point $R_{sh} = 20, n = 3$ on the domain's boundary. This time however, $S_{min} = 1281$. The fact $f(0.02, R_{sh}, n)$ has overall lower values with respect to $f(0.04, R_{sh}, n)$ suggests that R_s optimal value is somewhat closer to $0.02[\Omega]$.

The impact that the diode-factor n has on the objective function is clearly visible in Fig. 3(a) and (b). Experimenting with the Newton–Raphson method later on, it was found that the iterative process is indeed highly sensitive to small changes in n. Consequently, an inappropriate value of n attained in some iterative step in the course of the optimization process was very likely to lead to the divergence of the algorithm.

In order to address the latter difficulty, the classical Newton–Raphson method in (4.6) was extended with an additional stage. The extended Newton–Raphson method is depicted graphically as a flow-chart in Fig. 4. The modified algorithm starts with an initial parameters vector $\underline{\beta_0}$, whose elements are recovered from the

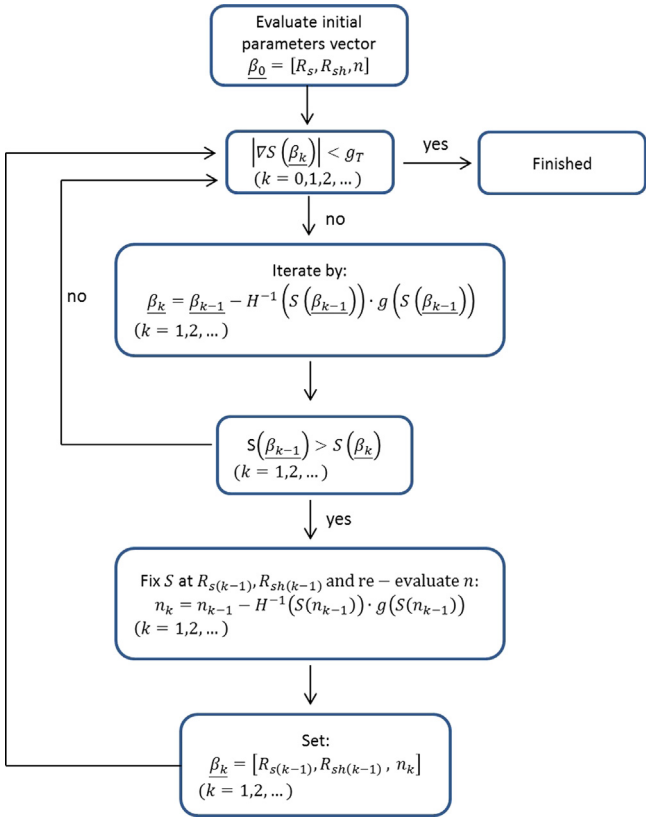

Fig. 4. Flow chart of the extended Newton–Raphson method.

experimental I–V characteristics through Eq. (3.3). Exceptional is the choice for the initial value of n – as a rule of thumb, $n^{(0)}$ shall be equal to 1.5 for Si cells, and 2.5 for Multi-junction cells. At each iterative step, Eq. (4.6) is applied. If however, at the end of the kth step, the objective function $f(\underline{\beta_k})$ has been increased compared to its previous $(k-1)^{th}$ value, then the following procedure is taken – f is fixed at its previous values, i.e., at $\{R_s^{(k-1)}, R_{sh}^{(k-1)}\}$, therefore transforming f into a function of one variable, $f(n)$. Next, a single-step of a Newton–Raphson iteration is applied on $f(n)$ so as to find an improved value for n (denoted n_k). The iterative process in Eq. (4.6) is then effectively re-initiated from the $(k-1)$th step, only with an improved version, n-wise, of the previously used $\underline{\beta_{k-1}}$, namely $\underline{\beta_{k-1}^{new}} = [R_s^{(k-1)}, R_{sh}^{(k-1)}, n_k]$. The entire process terminates when the magnitude of the objective function's gradient, $|\nabla f(\underline{\beta})|$, falls below a predefined limit.

5. Parameters extraction with the Levenberg–Marquardt method combined with Lambert-W function

The lambert-W function [11] is a set of functions, namely the branches of the inverse relation of the function $f(w) = w \cdot \exp(w)$, where w is any complex number. In other words, the defining equation for the Lambert W function is

$$z = W(z) \cdot \exp(W(z)) \tag{5.1}$$

The function $W(z)$ is multivalued. If we restrict our attention to real-valued $W(z)$ then this function is defined only for $z > -1/e$, and is double valued on the interval $(-1/e, 0)$. If we further impose another constraint $W(z) > -1$, then two branches of $W(z)$, denoted $W_0(z)$ and $W_{-1}(z)$, are defined. In Fig. 5 which shows $W(z)$ in $z \in [-0.5, 3]$, it can be seen that the upper branch,

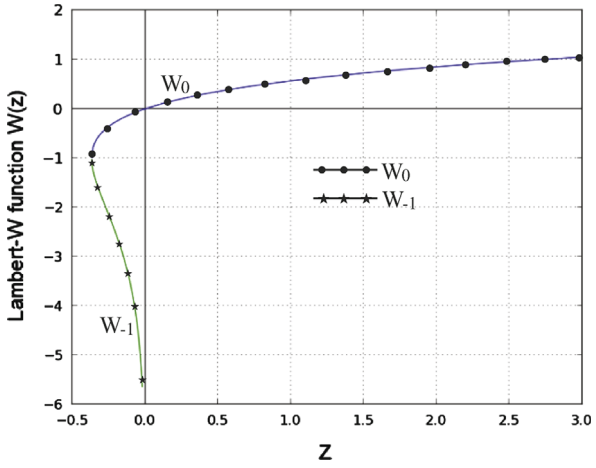

Fig. 5. The Lambert-W function, $W(z)$, with its 2 branches W_0 and W_{-1} specified.

$W_0(z)$, satisfies $W_0(0)=0$ and $W_0(-1/e)=-1$, while the lower branch, $W_{-1}(z)$, satisfies $W_{-1}(-1/e)=-1$ and decreases to $W_{-1}(0^-)\to\infty$.

By implicit differentiation (a differentiation of $W(z)$ is used when a gradient-descent method is employed), it is simple to show that all the branches of $W(z)$ satisfy

$$\frac{dW}{dz}=\frac{W(z)}{z(1+W(z))},\quad z\notin\{0,-1/e\} \tag{5.2}$$

Equations that contain exponential terms can be solved using the Lambert W function. The general strategy is to rearrange an equation that includes an exponential and make it look like $y=x\cdot\exp(x)$, at which point a value for the unknown variable x is provided by W as follows:

$$y=x\cdot\exp(x)\Longrightarrow x=W(y) \tag{5.3}$$

Rearranging the non-linear Eq. (2.1) to isolate the terms where the current I appears, we have

$$I(1+R_s/R_{sh})+[V/R_{sh}-(I_0+I_L)]=-I_0\cdot\exp\left(\frac{V}{n\cdot V_T}\right)\cdot\exp\left(\frac{R_s}{n\cdot V_T}\cdot I\right) \tag{5.4}$$

To simplify the writing of (5.4), the terms of the equation are substituted with a single letter, namely

$$\alpha I+\beta=\gamma\cdot\exp(\delta\cdot I) \tag{5.5}$$

where, in Eq. (5.5), $\alpha=1+R_s/R_{sh}$, $\beta=[V/R_{sh}-(I_0+I_L)]$, $\gamma=-I_0\cdot\exp(V/n\cdot V_T)$, and $\delta=R_s/(n\cdot V_T)$.

It can be verified that Eq. (5.5) can be transformed via the substitution $z=\alpha I+\beta$ into

$$\left(-\frac{\delta}{\alpha}z\right)\cdot\exp\left(-\frac{\delta z}{\alpha}\right)=-\frac{\delta}{\alpha}\cdot\gamma\cdot\exp\left(-\frac{\delta\cdot\beta}{\alpha}\right) \tag{5.6}$$

Now, using Eq. (5.3), a solution for z is obtained:

$$z=-\frac{\beta}{\alpha}-\frac{1}{\delta}\cdot W\left(-\frac{\delta}{\alpha}\gamma\cdot\exp\left(-\frac{\delta\cdot\beta}{\alpha}\right)\right) \tag{5.7}$$

which, upon writing z back in terms of I, and re-assigning α, β, γ and δ, gives

$$I(V,R_s,R_{sh},n,I_0,I_L)=\frac{(I_L+I_0)-V/R_{sh}}{1+R_s/R_{sh}}-\left(\frac{R_s}{n\cdot V_T}\right)^{-1}\times W\left\{\frac{\left(\frac{R_s\cdot I_0}{n\cdot V_T}\cdot\exp\left(\frac{V}{n\cdot V_T}\right)\right)}{1+R_s/R_{sh}}\cdot\exp\left[\frac{R_s/(n\cdot V_T)}{1+R_s/R_{sh}}\cdot\left[I_L+I_0-\frac{V}{R_{sh}}\right]\right]\right\} \tag{5.8}$$

Hence, the Lambert W function enables the writing of Eq. (2.1) in an *explicit form* $I=f(V)$.

The number of unknown parameters in Eq. (5.8) can be reduced from 5 to 3 by substituting I_0 and I_0+I_L with Eqs. (2.4) and (2.5) respectively, giving

$$I(V,R_s,R_{sh},n)=A_1-A_2\cdot W\{A_3\cdot\exp(A_4)\} \tag{5.9}$$

where

$$A_1(R_s,R_{sh},n)=\frac{\frac{I_{sc}(1+R_s/R_{sh})-V_{oc}/R_{sh}}{1-\exp\left(\frac{R_s\cdot I_{sc}-V_{oc}}{n\cdot V_T}\right)}+\frac{V_{oc}}{R_{sh}}-\frac{V}{R_{sh}}}{1+R_s/R_{sh}} \tag{5.9a}$$

$$A_2(R_s,R_{sh},n)=\left(\frac{R_s}{n\cdot V_T}\right)^{-1} \tag{5.9b}$$

$$A_3(R_s,R_{sh},n)=\frac{\left(\frac{R_s}{n\cdot V_T}\cdot\exp\left(\frac{V}{n\cdot V_T}\right)\right)}{1+R_s/R_{sh}}\cdot\frac{\left[I_{sc}(1+R_s/R_{sh})-V_{oc}/R_{sh}\right]\cdot\exp\left(-\frac{V_{oc}}{n\cdot V_T}\right)}{1-\exp\left(\frac{R_s\cdot I_{sc}-V_{oc}}{n\cdot V_T}\right)} \tag{5.9c}$$

$$A_4(R_s,R_{sh},n)=\frac{\frac{R_s}{n\cdot V_T}}{1+R_s/R_{sh}}\left[\frac{I_{sc}(1+R_s/R_{sh})-V_{oc}/R_{sh}}{1-\exp\left(\frac{R_s\cdot I_{sc}-V_{oc}}{n\cdot V_T}\right)}+V_{oc}/R_{sh}-V/R_{sh}\right] \tag{5.9d}$$

Algebra-wise, Eq. (5.9) together with its sub-components (5.9a), (5.9b), (5.9c) and (5.9d), may seem rather complicated. However, bearing in mind that no assumptions or approximations were made in the derivation of Eq. (5.9), it can be asserted that Eq. (5.9) is an accurate expression for $I(V)$.

In the fitting process between the proposed model in Eq. (5.9) and the experimental solar cell I–V curves, an objective function is being minimized in terms of least-squares. Since Eq. (5.9) is explicit, the model consists of a single independent variable V in the right side of Eq. (5.9), hence the fitting process is one-dimensional.

As before, we denote $\underline{I}=\{I_k\}_{k=1..N}$ the N measured experimental current values, corresponding to N voltage measuring points $\underline{V}=\{V_k\}_{k=1..N}$. The current-voltage relation (5.9) can be written for each data sample as $I_k=f(V_k,\underline{\beta})$, where $\underline{\beta}$ is a set of unknown parameters (namely, R_s, R_{sh} and n). As before, the fitting process is based on finding $\underline{\beta}$ which minimizes the objective function $S(\underline{\beta})=\sum_{k=1}^{N}[I_k-f(V_k,\underline{\beta})]^2$.

$\underline{\beta}$ is optimized by the Levenberg–Marquardt algorithm (LMA) [12], which outperforms simple gradient-descent and other gradient methods in a wide variety of problems. Unlike the Newton–Raphson method, the LMA ordinarily finds a solution even if it starts far off the objective function's extremum. The LMA, like other gradient-descent based methods, requires an initial assigning for $\underline{\beta}$. In each iterative step, $\underline{\beta}$ is updated by a new estimate, $\underline{\beta}+\underline{\delta\beta}$, such that

$$S(V_k,\underline{\beta}+\underline{\delta\beta})\approx S(V_k,\underline{\beta})+\frac{\partial S(V_k,\underline{\beta})}{\partial\underline{\beta}}\cdot\underline{\delta\beta} \tag{5.10}$$

We denote by $\underline{J_k}$ the gradient of f w.r.t $\underline{\beta}$, i.e.,

$$\underline{J_k}=\frac{\partial f(V_k,\underline{\beta})}{\partial\underline{\beta}}=\left[\frac{\partial f(V_k,\underline{\beta})}{\partial R_s},\frac{\partial f(V_k,\underline{\beta})}{\partial R_{sh}},\frac{\partial f(V_k,\underline{\beta})}{\partial n}\right].$$

At its minimum, $S(\underline{\beta})$ satisfies $\forall k:\underline{J_k}=\underline{0}$. From Eq. (5.10), $S(\underline{\beta}+\underline{\delta\beta})\approx\sum_{k=1}^{N}[I_k-f(V_k,\underline{\beta})-\underline{J_k}\cdot\underline{\beta}]^2$.

Alternatively, in a vector notation:

$$S(\underline{\beta}+\underline{\delta\beta})=\|\underline{I}-\underline{f}(\underline{V})-\underline{J}(\underline{\beta})\cdot\underline{\beta}\|^2 \tag{5.11}$$

Taking the derivative of Eq. (5.11) w.r.t. δ and setting the result to zero, gives

$$(\underline{J}^T\underline{J})\cdot\underline{\delta\beta}=\underline{J}^T\{\underline{I}-\underline{f}(\underline{V})\} \tag{5.12}$$

where $\underline{J}$ in Eq. (5.12) is the Jacobian matrix of f, whose kth row equals $\underline{J}_k$, that is

$$\underline{J}=\begin{bmatrix} \frac{\partial f(V_1)}{\partial R_s} & \frac{\partial f(V_1)}{\partial R_{sh}} & \frac{\partial f(V_1)}{\partial n} \\ \frac{\partial f(V_2)}{\partial R_s} & \frac{\partial f(V_2)}{\partial R_{sh}} & \frac{\partial f(V_2)}{\partial n} \\ \cdot & \cdot & \cdot \\ \cdot & \cdot & \cdot \\ \frac{\partial f(V_N)}{\partial R_s} & \frac{\partial f(V_N)}{\partial R_{sh}} & \frac{\partial f(V_N)}{\partial n} \end{bmatrix} \tag{5.13}$$

Levenberg and Marquardt introduced a "damped version" of Eq. (5.12), replacing it with

$$(\underline{J}^T\underline{J}+\lambda\cdot diag[\underline{J}^T\underline{J}])\cdot\underline{\delta\beta}=\underline{J}^T\{\underline{I}-\underline{f}(\underline{V})\} \tag{5.14}$$

where $\lambda>0$ in Eq. (5.14) is the damping factor, adjusted at each iteration, and $diag\,[\underline{J}^T\underline{J}]$ is a diagonal matrix that consists of the diagonal elements of $\underline{J}^T\underline{J}$.

Roughly speaking, the intuition behind (5.14) is that λ dictates the rate of the convergence of LMA. If the reduction of $S(\underline{\beta})$ is fast, a smaller value of λ can be used, whereas if at each iteration $S(\underline{\beta})$ is being insufficiently reduced, then λ is increased and the iterative step will be approximately in the direction of the gradient. The iteration stops when either the length of the calculated step $\underline{\delta\beta}$ or the reduction in $S(\underline{\beta})$ fall below some predifined limits.

6. Parameters extraction with a Genetic-Algorithm

"Inspired" by the process that drives biological evolution, the genetic algorithm at each step employs a random selection of individuals, known as "parents", from a current population of solutions [14,15,16]. A solution in our terms refers to a vector of $[R_s, R_{sh}, n]$. The parental solutions produce the children for the next step of the algorithm by introducing changes into some of the current solutions (*mutation*), or by combining two current solutions so as to form newly improved ones (*crossover*). The underlying idea is that over successive generations, the initial population evolves toward an optimal solution.

The key operators involved in the GA are hereby described:

1. *Selection*: In each step, the algorithm ranks and picks the best solutions (referred to as "chromosomes" in GA terminology) of the current population and discard the least successful ones. The fittest solutions of the current generation reproduce the next generation of solutions.
2. *Reproduction*: An operation that takes two selected chromosomes (i.e., solutions) in the current population and crosses them to obtain new individuals. The most common type of crossing is a swap between corresponding genes (i.e., parameters) of two parental chromosomes. In parameters-extraction sense, a parent chromosome may consist, for instance, of 3 genes, namely R_s, R_{sh} and n.
3. *Mutation*: An operation that introduces a change in some of the genes of the chromosomes (i.e., the solutions) in a population. The mutation rate accounts for the percentage of chromosomes being mutated (rated between 1% and 20% of the current population).

The GA typically begins with a randomly selected population of chromosomes, where different genes of each chromosome in the solution domain are encoded as bits or numbers. A fitness-function (i.e., an objective function that one wishes to minimize, such as $S(\underline{\beta})$) is used in order to measure the quality of the chromosome-represented solution.

The genetic-algorithm is conceptually different from the two methods discussed previously, in the following aspects:

- *Search-wise*: The GA is *global* in its search, that is, eventually, no local minima solutions of the fitness function are obtained. Moreover, the starting points for the GA do not have a critical role in the convergence of the algorithm. The initial population hence can be entirely random or consists of known approximate solutions.
- *The solution domain*: The Newton–Raphson and the LMA start from a single point and progress until an optimal solution is achieved. The GA generates a "population" of points and terminates when either a maximum number of generations has been reached or when the value of the fitness function for the 'best' point in the current population is less than or equal to some fitness limit.
- *Mathematical-wise*: Obtaining the optimal solution does not require the derivative of the fitness function.
- *Procedure-wise*: Unlike the deterministic nature of the Newton–Raphson and the LMA methods, the GA employs probabilistic rules and random choices. For instance, many *selection* rules employ a "roulette wheel" mechanism to probabilistically select individuals in a population based on their performance. Roughly speaking, a roulette mechanism simulates a roulette wheel with an area of each segment of the roulette corresponding to a single individual in the current population. An individual in a population that has a good fitness occupies a larger area within the roulette and has a better chance to be selected as a parent for the reproduction of the next generation.

It should also be noted that in the GA case, Eq. (4.4) agrees with the fitness-function discussed earlier.

7. Extraction results and discussion

As aforesaid, two types of cells, namely Si and Multi-junction cells, were examined. Each type consisted of a different number of data samples ranging from 90 to a little more than 200. All Si cells were originally tested at 25 °C, 1*Sun*, whereas the MJ cell[1] was tested at 80 °C, and under three concentration values of 350, 555 and 750 Sun. As there is no prior knowledge of the parameters true value, the extraction error serves as a the principal measure for the quality of the extraction. The extraction error criterion, ε, shall be defined as

$$\varepsilon=\frac{\sum_{k=1}^{N}(I_{measured}[k]-I_{theoretical}[k])^2}{\sum_{k=1}^{N}(I_{measured}[k])^2} \tag{7.1}$$

that is, ε is the sum of squared difference between the experimental and the theoretical modeled current samples, normalized by the sum of squared experimental currents samples. Since extraction results are quite similar for all methods, a secondary criterion for electing the preferred method may be the ACT - the Algorithm Conversion Time, or the elapsed running time of the algorithm associated with the method.

Table 1 specifies the parameters initial values of all cells, that are inserted into the NRM and the LMA. Initial values for the resistances and the diode-ideality factor have been calculated in Section 3, whereas initial values for the reverse and the photo-

[1] Data provided courtesy of Spectrolab Inc.

generated currents were derived indirectly from Eqs. (2.4) and (2.5). The GA does not require initial values. However, some prerequisite settings of the algorithm should be made to insure proper results. For instance, the solutions for the Si and the MJ cells were restricted by lower and upper bounds so as to limit the global search into a predefined domain. In the Si case, lower and upper bounds were fixed at [0, 0, 1] and [0.1, 10, 2], respectively. Likewise, MJ population was confined between [0, 0, 2] and [0.05, 1000, 3].

The *population size* in both cases (Si and MJ) was set to 150 individual solutions, in which case the GA's *elite-count,* i.e., the number of individuals that are guaranteed to survive to the next generation, was assigned 20. The *crossover-fraction,* that is, the fraction of the next generation that is produced by the *reproduction* operation (see Section 6), was set to 0.8. The selection operation is subjected to a probabilistic selection function that is based on the individuals value of the fitness function. We chose to apply the *Roulette* selection function [13].

Table 1
Si and MJ cells initial parameters value for the Newton–Raphson and Levenberg–Marquardt methods.

Solar cell	$R_s^{(0)}$ (Ω)	$R_{sh}^{(0)}$ (Ω)	$n^{(0)}$	$I_0^{(0)}$ (A)	$I_L^{(0)}$ (A)
Si1	0.0087	2.6379	1.5	4.0763×10^{-7}	2.6075
Si2	0.0089	3.6060	1.5	3.5714×10^{-7}	2.5954
Si3	0.0094	5.3347	1.5	4.4369×10^{-7}	2.5898
MJ(350Sun)	0.0372	112.95	2.5	5.6283×10^{-28}	4.4773
MJ(555Sun)	0.0267	117.56	2.5	5.4108×10^{-28}	7.0764
MJ(750Sun)	0.0372	112.95	2.5	2.5521×10^{-28}	8.8495

Table 2
Parameters extraction results from a noisy I–V Data – Si cells.

Solar cell	Method	R_s (Ω)	R_{sh} (Ω)	n	I_0 (μA)	I_L (A)	ε $(\times 10^{-6})$	ACT (sec)
Si1	NRM[a]	0.0034	2.771	1.7257	3.1355	2.6107	6.596	371
	LMA[b]	0.0031	2.771	1.7386	3.4753	2.6109	6.2599	4
	GA[c]	0.0035	2.799	1.7217	3.0405	2.6094	6.7456	31
Si2	NRM	0.0012	2.698	1.8627	7.4917	2.5898	17.970	374
	LMA	0.0012	2.699	1.8627	7.4417	2.5954	9.966	3
	GA	0.0014	2.932	1.8690	7.8251	2.5847	14.496	31
Si3	NRM	0.0032	5.292	1.7957	5.7174	2.5831	10.912	377
	LMA	0.0028	5.266	1.8109	6.3921	2.5837	8.515	4
	GA	0.0028	5.283	1.8129	6.4850	2.5836	8.513	32

[a] Newton–Raphson Method.
[b] Levenberg–Marquardt Algorithm.
[c] Genetic-Algorithm.

The first stage of the extraction included the experimental I–V characteristics of the Si and the MJ cells which contained measurements noise. Results in both cases are reported in Tables 2 and 3. The results in Table 3 may serve as an indicator, in terms of solar cell physics, to the quality of the extraction. As the concentration is increased from 350 to 750 Sun, the series resistance, R_s is expected to decrease. Indeed, the R_s values seem to agree with the latter assumption throughout all three methods. In contrast, the values of R_{sh} are much less consistent, since they do not to decrease with the concentration as one would expect. The instability of the results for the shunt resistance can be attributed in part to the measurements noise. It is mainly important to note that the shunt resistance is large enough to be considered negligible in the MJ case. This fact was later verified by replacing the extracted R_{sh} with another high value, in the order of 10^2. After replacement, the error remained in the order of 10^{-6}, indicating how little effect R_{sh} has on the I–V characteristics of the examined MJ cell. Note however, that in the Si case, the results for R_{sh} are moderate in magnitude and show a consistency throughout all three methods. The diode ideality factor, n, is expected to increase with the rise of the concentration. This demand is met only by the first and the third concentration values. The second 555Sun results show a decrease in n throughout all methods. This can be accounted again for the measurements noise that is involved in the MJ's second dataset. Alternatively, it can be asserted that the MJ cell's 555Sun measurements were taken inappropriately and that the experiment should be repeated. The reverse saturation current, I_0, is also expected to increase with the concentration. However, since from Eq. (2.4) I_0 is dependent on R_{sh} and n, it fails to follow any pattern of increase.

After extracting the solar cells parameters, synthetic I–V characteristics can be generated based on the single-diode model Eq. (2.1). Synthetic I–V curves are naturally devoid of any measurement noises, and may therefore serve to re-examine the parameters extraction. In Tables 4 and 5, the parameters extraction results are reported for the Si cells and the MJ cell, respectively. For every cell, each extraction methods is re-applied on each of the synthetic I–V curves, previously generated by every algorithm. For instance, in Table 4, the entry "NRM of LMA" in the second column that is related to the Si1 cell, indicates that the NRM method is used to extract parameters from the synthetic I–V data, which is itself generated by the implementation of the LMA on the original noisy data.

Naturally, in Table 5 the parameters R_{sh} and n do not correlate with the concentration, as the synthetic I–V curve is merely derived from the noisy data. However, unlike Tables 2 and 3, the results in Tables 4 and 5 are far more distinct in terms of the extraction error. In Table 5, the extraction error that is obtained by applying the NRM is on average 10^3 and 10^7 times lower than the

Table 3
Parameters extraction results from a noisy I–V Data – multi-junction cells.

Concentration	Method	R_s (Ω)	R_{sh} (Ω)	n	I_0 $(\times 10^{-16} A)$	I_L (A)	ε $(\times 10^{-6})$	ACT (sec)
350Sun	NRM[a]	0.0254	576	2.6329	5.7075	4.4775	87.171	1376
	LMA[b]	0.0255	170	2.6114	4.2118	4.4780	86.150	16
	GA[c]	0.0245	72	2.6402	6.3818	4.4913	76.770	42
555Sun	NRM	0.0179	191	2.5617	2.4346	7.0771	388.83	1383
	LMA	0.0171	435	2.5212	1.4116	7.0680	258.43	11
	GA	0.0187	455	2.5529	2.0868	7.0723	599.12	45
750Sun	NRM	0.0141	222	2.6901	1.0786	8.8538	152.06	1401
	LMA	0.0140	159	2.7066	13.4720	8.8503	155.94	5
	GA	0.0145	156	2.6238	4.2322	8.8503	194.68	45

[a] Newton–Raphson Method.
[b] Levenberg–Marquardt Algorithm.
[c] Genetic-Algorithm.

Table 4
Parameters extraction results from a smooth I–V Data – Si cells.

Solar cell	Method	R_s (Ω)	R_{sh} (Ω)	n	I_0 (μA)	I_L (A)	ε	ACT (sec)
Si1	NRM of NRM	0.0034	2.768	1.7245	3.1053	2.6108	3.45×10^{-9}	128
	NRM of LMA	0.0031	2.769	1.7379	3.4550	2.6109	1.08×10^{-9}	400
	NRM of GA	0.0035	2.796	1.7206	3.0132	2.6095	2.74×10^{-9}	312
	LMA of NRM	0.0034	2.771	1.7262	3.1484	2.6107	2.29×10^{-9}	4
	LMA of LMA	0.0031	2.772	1.7388	3.4810	2.6109	2.11×10^{-9}	4
	LMA of GA	0.0035	2.798	1.7214	3.0333	2.6094	4.88×10^{-10}	4
	GA of NRM	0.0036	2.770	1.7172	2.9319	2.6109	2.65×10^{-7}	37
	GA of LMA	0.0032	2.762	1.7325	3.3136	2.6110	2.52×10^{-8}	36
	GA of GA	0.0037	2.781	1.7098	3.8151	2.6131	7.02×10^{-8}	30
Si2	NRM of NRM	0.0015	2.683	1.8478	6.7480	2.5902	5.01×10^{-7}	413
	NRM of LMA	0.0017	2.678	1.8406	6.3678	2.5960	1.02×10^{-6}	374
	NRM of GA	0.0012	2.654	1.8398	6.5455	2.5912	3.72×10^{-7}	319
	LMA of NRM	0.0012	2.698	1.8623	7.4687	2.5898	5.68×10^{-10}	5
	LMA of LMA	0.0012	2.698	1.8610	7.3549	2.5954	3.76×10^{-9}	3
	LMA of GA	0.0011	2.671	1.8666	7.4250	2.5847	7.25×10^{-9}	4
	GA of NRM	0.0015	2.723	1.8513	6.9228	2.5901	7.75×10^{-7}	33
	GA of LMA	0.0012	2.706	1.8657	7.5957	2.5954	5.91×10^{-8}	29
	GA of GA	0.0016	2.916	1.8585	7.2832	2.5848	9.52×10^{-8}	30
Si3	NRM of NRM	0.0034	5.247	1.7857	5.3099	2.5833	2.19×10^{-7}	423
	NRM of LMA	0.0030	5.224	1.8022	5.9967	2.5839	1.79×10^{-7}	356
	NRM of GA	0.0030	5.241	1.8042	6.0861	2.5838	1.71×10^{-7}	374
	LMA of NRM	0.0032	5.291	1.7959	5.7240	2.5831	2.27×10^{-9}	4
	LMA of LMA	0.0028	5.264	1.8109	6.3935	2.5837	8.33×10^{-10}	4
	LMA of GA	0.0028	5.279	1.8120	6.4454	2.5836	1.46×10^{-9}	3
	GA of NRM	0.0030	5.432	1.8111	6.3901	2.5829	1.85×10^{-7}	33
	GA of LMA	0.0026	5.388	1.8284	7.2368	2.5835	1.71×10^{-7}	37
	GA of GA	0.0028	5.290	1.8153	6.5965	2.5836	7.87×10^{-8}	31

Table 5
Parameters extraction results from a smooth I–V Data – multi-junction cells.

Concentration	Method	R_s (Ω)	R_{sh} (Ω)	n	I_0 ($\times10^{-16}A$)	I_L (A)	ε	ACT (sec)
350Sun	NRM of NRM	0.0255	568	2.6288	4.8081	4.4778	5.09×10^{-13}	1458
	NRM of LMA	0.0256	173	2.6181	4.0147	4.4773	7.73×10^{-13}	1398
	NRM of GA	0.0247	74	2.6468	5.3518	4.4978	5.16×10^{-13}	42
	LMA of NRM	0.0253	570	2.6364	5.3841	4.4713	1.35×10^{-12}	9
	LMA of LMA	0.0253	165	2.6148	4.0025	4.4713	1.56×10^{-9}	10
	LMA of GA	0.0244	74	2.6451	5.8213	4.4996	1.24×10^{-10}	8
	GA of NRM	0.0252	568	2.6289	1.2581	4.4801	1.25×10^{-8}	46
	GA of LMA	0.0250	165	2.6213	5.9912	4.4685	2.25×10^{-7}	44
	GA of GA	0.0242	80	2.6351	5.8123	4.4877	1.25×10^{-7}	42
550Sun	NRM of NRM	0.0180	188	2.5539	2.4346	7.0771	9.10×10^{-13}	1403
	NRM of LMA	0.0173	173	2.5246	1.7221	7.0645	3.68×10^{-14}	1412
	NRM of GA	0.0185	451	2.5537	3.3715	7.0737	1.68×10^{-13}	45
	LMA of NRM	0.0177	188	2.5693	2.6842	7.0737	9.62×10^{-13}	12
	LMA of LMA	0.0168	437	2.5293	1.9521	7.0656	1.99×10^{-9}	10
	LMA of GA	0.0191	448	2.5573	2.8427	6.9852	3.90×10^{-10}	7
	GA of NRM	0.0176	187	2.5733	4.2541	7.0801	6.52×10^{-8}	41
	GA of LMA	0.0176	429	2.5158	2.2515	7.0800	4.25×10^{-8}	50
	GA of GA	0.0179	448	2.5488	1.7121	7.0698	9.22×10^{-7}	45
750Sun	NRM of NRM	0.0140	219	2.6913	10.786	8.8538	1.52×10^{-13}	1512
	NRM of LMA	0.0138	161 e	2.7093	11.8315	8.8524	2.67×10^{-13}	1377
	NRM of GA	0.0147	153	2.6291	3.9631	8.8591	6.36×10^{-13}	45
	LMA of NRM	0.0142	224	2.6943	19.364	8.8592	1.84×10^{-11}	9
	LMA of LMA	0.0138	155	2.7016	11.582	8.8573	3.33×10^{-9}	9
	LMA of GA	0.0143	156	2.6263	3.8562	8.8080	1.02×10^{-10}	7
	GA of NRM	0.0134	225	2.6811	20.515	8.8121	4.88×10^{-8}	46
	GA of LMA	0.0136	154	2.7877	9.2541	8.7354	4.44×10^{-8}	44
	GA of GA	0.0150	150	2.6301	3.5974	8.8430	6.66×10^{-7}	45

errors obtained by the LMA and the GA, respectively. On the other hand, similar to Tables 2 and 3 is the scale of the extraction running time – the ACT. Throughout all extractions, the NRM seems to consume the longest amount of computation time. This can be explained by the fact that we have generated our own code for the NRM in the Matlab environment, so as to insert variations into the original algorithm, disregarding aspects of code complexity. The self-written code has enabled us to control the rate of the convergence of the NRM, which in turn contributed to the extremely low errors. In contrast, the LMA and the GA were applied using the Matlab toolbox. Such toolbox may incorporate a fast converging functions but it is based on an inaccessible code.

8. Conclusions

In this work, three mathematical techniques were implemented to extract the physical parameters of solar cells based on the single-diode model. To do so, experimental Si and MJ solar cells data were used. These experimental samples contained measurement errors and data noise whose impact on the extraction results had to be considered and examined. Of special interest was the MJ cell, whose I–V characteristics were generated by testing the cell with an increasing concentration. The extraction results of the MJ cell were counter-intuitive, as the extracted values of the shunt resistance, R_{sh}, and of the diode ideality factor, n, failed to exhibit any consecutive pattern that correlated with the concentration. This inconsecutive pattern repeated itself throughout all three methods. We thus concluded that the 555 Sun measurements were either inappropriately taken, or that an excess measurement noise had been the cause for non-realistic results. It is therefore remained inconclusive whether one technique surpasses the others in terms of the extraction accuracy. It can be ascertained however, that if solar cells manufacturers wish to estimate their cell parameters via curve-fitting techniques, measurements need to be taken with utmost sensitivity to possible errors. The extraction was then repeated with smooth synthetic I–V curves, by cross-extracting the parameters of each synthetic data with each method. The extraction results for the synthetic MJ cells showed that the error obtained by the NRM was considerably lower than the other two methods. This low error implies that although the NRM is less convenient in terms of convergence rate, it may still be considered favorable over the LMA and the GA.

Acknowledgment

The authors wish to acknowledge Spectrolab Inc. for providing solar cell data.

References

[1] A. Ben-Or, J. Appelbaum, Estimation of multi-junction solar cell parameters, Progr. Photovolt.: Res. Appl. 21 (2013) 713–723.
[2] F. Ghani, M. Duke, Numerical determination of parasitic resistances of a solar cell using the Lambert-W function, Solar Energy 85 (2011) 2386–2394.
[3] D.S.H. Chan, J.R. Phillips, C.H. Phang, A comparative study of extraction methods for solar cell model parameters, Solid State Electron. 29 (1986) 329–337.
[4] J. Appelbaum, A. Chait, D. Thompson, Parameter estimation and screening of solar cells, Progr. Photovolt.: Res. Appl. 1 (1993) 96–103.
[5] S. Yadir, M. Benhmida, M. Sidki, A.E. Elmahdi, M. Khaidar, New method for extracting the model physical parameters of solar cells using explicit analytic solutions of current–voltage equation, in: International Conference on Microelectronics, Marrakech, Morocco, 2009, pp. 390–393.
[6] M. Ye, X. Wang, X. Yousheng, Parameter extraction of solar cells using particle swarm optimization, J. Appl. Phys. 105 (2009) 094502.
[7] A. Maoucha, F. Djeffal, D. Arar, N. Lakhdar, T. Bendib, M.A. Abdi, An accurate Organic solar cell parameters extraction approach based on the illuminated I–V characteristics for double diode modeling, in: First International Conference on Renewable Energies and Vehicular Technology, Hammamet, Tunisia, 2012, pp. 74–77.
[8] D. Chan, J. Phang, Analytical methods for the extraction of solar-cell single and double-diode model parameters from I–V characteristics, IEEE Trans. Electr. Dev. 34 (1987) 286–293.
[9] A. Sellami, M. Bouaicha, Application of the genetic algorithms for identifying the electrical parameters of PV solar generators, in: L.A. Kosyachenko (Ed.), Solar Cells – Silicon Wafer-Based Technologies, 2011, pp. 349–364.
[10] M. Wolf, G.T. Noel, J.R. Stirn, Investigation of the double exponential in the current–voltage characteristics of silicon solar cells, IEEE Trans. Electr. Dev. 24 (1977) 419–428.
[11] Lambert W function, Retrieved February 2013, from the Electronic-reference: ⟨http://en.wikipedia.org/wiki/Lambert_W_function⟩.
[12] Levenberg–Marquardt algorithm, Retrieved February 2013, from the Electronic-reference ⟨http://en.wikipedia.org/wiki/Levenberg%E2%80%93Marquardt_algorithm⟩.
[13] A. Chipperfield, P. Fleming, P. Hartmut, C. Fonseca, Genetic-Algorithm toolbox for use with Matlab - Version 1.2 User's Guide 2004; chap.1(2004) 1–11. Available via: ⟨http://crystalgate.shef.ac.uk/code/manual.pdf⟩.
[14] A. Zagrouba, A. Sellami, M. Bouaicha, M. Ksouri, Identification of PV solar cells and modules parameters using the genetic algorithms: appliction to maximum power extraction, Sol. Energy 84 (2010) 860–866.
[15] J. Jervase, H. Bourdoucen, A. Al-Lawati, Solar cell parameter extraction using genetic algorithms, Meas. Sci. and Technol. 12 (2001) 1922–1925.
[16] N. Moldovan, R. Picos, M.E. Garcia, Parameter extraction of a solar cell compact model using genetic algorithms, in: Proceedings of the 2009 Spanish Conference on Electron Devices (2009), Santiago de Campostela, Spain, pp. 379–382.